Highly-efficient hybrid white organic light-emitting diodes based on a high radiative exciton ratio deep-blue emitter with improved concentration of phosphorescent dopant†

Xinhua Ouyang,[a] Xiang-Long Li,[b] Yongqi Bai,[a] Dongbo Mi,[a] Ziyi Ge*[a] and Shi-Jian Su*[b]

An improved concentration of phosphorescent dopant for highly-efficient hybrid white organic light-emitting diodes based on a high radiative exciton ratio (80%) deep-blue emitter has been developed. The high radiative exciton ratio for the deep-blue emitter was found to be the transfer from the higher triplet (T_5) to the lowest singlet state (S_1) by a "hot-exciton" process. Notably, when the concentration of Ir(2-phq)$_3$ is up to 0.9 wt%, the OLED still exhibited white emission with a maximum total EQE, CE and PE of 22.3%, 53.7 cd A^{-1} and 60.2 lm W^{-1}, respectively. The exciton transfer mechanism in a high concentration of phosphorescent dopant was also discussed. The studies provide a way to obtain high performance F/P hybrid WOLEDs with a simple architecture and improved doping concentration.

1. Introduction

White organic light-emitting diodes (WOLEDs) have been attracting great attention due to their favorable properties of good color rendering, flexibility, and homogenous large-area emission for lighting sources and full color OLEDs.[1–4] In the past two decades, some effective approaches have been used to achieve WOLEDs including full fluorescent,[5] phosphorescent[6] and hybrid WOLEDs.[7] Generally, for the full fluorescent WOLEDs, they have been demonstrated with excellent stability. However, these devices show low efficiencies owing to the limit of exciton statistics.[8] So, in order to obtain high efficiencies, the researchers begin to focus on the full phosphorescent WOLEDs, which have been reported with high efficiencies up to 100% internal quantum efficiency. Unfortunately, these devices are not stable enough to ensure a long device life-time as the limit of the availability of high performance blue hosts/emitters.[9] Moreover, an intrinsic exchange energy loss arising from energy transfer from the host's singlets to the phosphorescent guest's triplets cannot be prevented fully. In view of this, the development of fluorescence (F) and phosphorescence (P) hybrid

WOLEDs is considered to be an ideal solution to approach high-efficiency and long life-time WOLEDs.

Commonly, the hybrid WOLEDs can be constructed using two architectures, including multi-emissive-layers (multi-EML), or a single-emissive-layer (single-EML) with different color emitting dopants. The multi-EML structure usually requires complexity of device fabrication with an interlayer between the fluorophore and phosphor to prevent mutual exciton transfer and quenching processes, which decrease the reproducibility and raise the fabrication cost. Furthermore, the complicated multilayer structure is also difficult to be achieved by solution processing. Compared to the multi-EML counterpart, the single-EML can be avoided effectively the accumulation of charges and the generation of a higher electric field at the interfaces, especially for the single-dopant single-EML WOLEDs. Therefore, the single-dopant single-EML structure is thought to be a potential strategy to fabricate hybrid WOLEDs with high efficiencies.

In the early work, Leo et al. demonstrated one kind of single-dopant single-EML F/P hybrid WOLEDs by doping a yellow phosphor (Ir(MDQ)$_2$(acac)) into a blue fluorescent host (4P-NPD).[10] Their exhibited external quantum efficiencies (EQEs) at a practical brightness of 1000 cd m^{-2} are much lower than the theoretically maximum EQE (EQE$_{max}$) of 20%, which can be attributed to the unipolar of 4P-NPD. And the corresponding power efficiencies are not yet high enough for practical applications. In the meantime, Ma et al. reported one of bipolar derivatives containing triphenylamine and oxadiazole units for single-dopant single-EML WOLEDs.[11] A maximum current efficiency (CE) of 7.9 cd A^{-1} (a corresponding EQE of 5.2%) was achieved. Most recently, higher

performance with maximum total EQE of 26.6%, total efficiencies of 53.5 cd A^{-1} and 67.2 lm W^{-1} has been obtained by Zhang's group based on a blue fluorophor (DADBT) and orange phosphors (Ir(2-phq)$_3$) hybrid single-dopant single-EML.[12] Nevertheless, the dopant concentration of phosphors in these WOLEDs with single-dopant single-EML structure was very low (0.1%), which was difficult to be controlled by vacuum deposition. Moreover, the color was very sensitive to the dopant concentration of phosphors. A small variation in the dopant concentration would result in a pronounced change in the energy transfer between the emitting dopants. Therefore, developments of improving dopant concentration design strategies for flexible manipulation have been considered as the current key challenges for progressing single-dopant single-EML F/P hybrid WOLEDs.

In this work, we demonstrated the first time with improved dopant concentration by design and synthesis of an ideal saturated deep-blue fluorophor, N,N-diphenyl-4″-(1,4,5-triphenyl-1H-imidazol-2-yl)-[1,1′:4′,1″-terphenyl]-4-amine (**DPTPA**), which exhibits high radiative exciton ratio and deep-blue emission. The single-dopant single-EML F/P hybrid WOLED has been fabricated with improved dopant concentration to 0.9%, which dose not follow the conventional principle of the doping concentration regulation. The device still shows white emission and excellent electroluminescence (EL) performance with a low turn-on voltage of 2.6 V, maximum total EQE, CE and PE of 22.3%, 53.7 cd A^{-1} and 60.2 lm W^{-1}, respectively.

2. Results and discussion

2.1 Synthesis and crystal structure

For the synthesis of **DPTPA** (Fig. 1), the important intermediate was 4″-(diphenyl-amino)-[1,1′:4′,1″-terphenyl]-4-carbaldehyde (**3**), which was synthesized by Suzuki couplings of 4′-bromo-N,N-diphenyl-[1,1′-biphenyl]-4-amine (**2**) and (4-formyl-phenyl) boronic acid using Pd(PPh$_3$)$_2$Cl$_2$ as catalysis. While compound **2** can be prepared by mixing (4-(diphenylamino) phenyl)boronic acid (**1**) and 1-bromo-4-iodobenzene in the presence of Pd(PPh$_3$)$_2$Cl$_2$, K$_2$CO$_3$ and toluene. Finally, the condensation of compound **3** and benzil resulted in the target
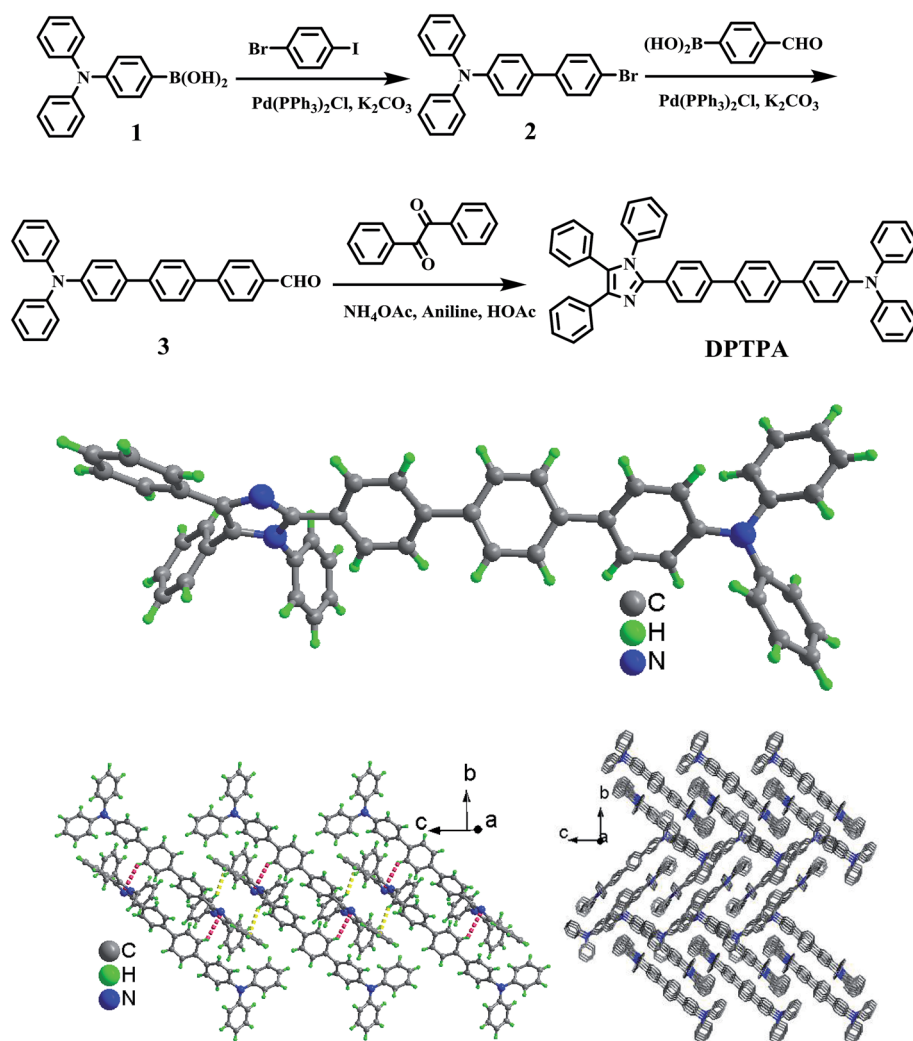

Fig. 1 The synthetic route and crystal structure of **DPTPA**.

compound **DPTPA** with high yield. Single-crystal of **DPTPA**† was obtained from a layering of ethanol onto a mixed solution of dichloromethane and *n*-hexane. As shown in the crystal structure, the highly twisted geometry is found in the **DPTPA** to contain *N*-substituted benzene ring with imidazole plane and triphenylamine (TPA) moiety in **DPTPA** with the imidazole plane, and the dihedral angles are 97.6° and 23.3°, respectively.

2.2 Electrochemical and thermal and properties

The electrochemical behavior of **DPTPA** was studied by cyclic voltammetry (CV). The HOMO level of **DPTPA** was determined from the onset potential of the first oxidation relative to ferrocene (Fig. 2a), and the LUMO level was calculated by adding the optical band gap to the HOMO levels. The results are summarized in Table 1. The first oxidation event is observed at 0.86 (*vs.* Fc/Fc$^+$). The potentials can be translated to HOMO level of 5.26 eV. The thermal properties of **DPTPA** were investigated with TGA and DSC under a nitrogen atmosphere as shown in Fig. 2b, and their thermal data are summarized in Table 1. The TGA measurement shows that **DPTPA** possesses high thermal stabilities of more than 400 °C. A weight loss of 5% (T_d) is observed at 469 °C. The value is more than 100 °C above the

Fig. 2 (a) The oxidation curve of DPTPA from cyclic voltammetry; (b) the TGA and DSC curves of DPTPA.

sublimation temperatures and therefore proves the high thermal stability. The DSC curve shows the glass-transition temperatures (T_g) is found to be 151 °C.

2.3 Theoretical calculation

The geometry and electronic structures of **DPTPA** were obtained using density functional theory (DFT) at the B3LYP/6-31G(d,p) level in the Gaussian 03 program.[13] The calculated dihedral angles between imidazole and *N*-substituted benzene ring and triphenylamine moieties are 87.8° and 41.5°, respectively. The large twisted geometry configuration might prevent intramolecular extending of π-electron and suppress molecular packing in the solid state effectively, which is agreement with the results of the crystal structure. The electron dentistry of **DPTPA** was shown in Fig. 3. The HOMO orbit of **DPTPA** mainly populate on the whole molecule, while the corresponding LUMO orbit mainly locate on the linker and imidazole moieties. A large overlapping was found in the molecule, which would be benefit to balance the carriers. The values of HOMO and LUMO levels are 4.9 eV and 2.24 eV, respectively. In contrast, the absolute values of the frontier orbital energies have a 0.36 eV discrepancy between the experimental and theoretical data. As DFT-calculations were performed in gas-phase only, solvent effects occurring during experimental characterization were not taken into account. Additionally, time-dependent (TD) DFT calculations were used to predict the lowest and higher exited states (triplets and singlets), two degenerate triplet levels (T_3 and T_4) of 3.007 eV, which is lower than the value of the S_1 level (3.267 eV). And the lower triplet states (T_1 and T_2) are 2.614 eV and 2.848 eV, respectively. All of these low triplet states are ascribed to the transition from HOMO−1 to LUMO and from HOMO−2 to LUMO+1, both located on the same imidazole unit. The transitions between spatially non-overlapped HOMO−2 and LUMO orbitals are ascribed to S_1 and T_5, and their energy difference is zero. HOMO−2 and LUMO+2 also do not overlap, and the transitions between them are ascribed to S_2 and T_9; their energy difference is also zero. These zero gaps between the exited singlet ($S_n \geq 1$) and triplet ($T_m \geq 3$) state may offer some advantage with respect to increasing the radiative singlet-state population from the nonradiative high triplet state, generated by the "hot-exciton" process from the T_5 to S_1 states.

2.4 Absorption and photoluminescent properties

The absorption and photoluminescent (PL) spectra in film and solution are shown in Fig. 4. The absorption spectra in solution and film are nearly identical, implying small dipolar changes at the ground state in different surroundings. The absorptive spectra is characterized by an absorption maximum at $\lambda_{max,abs}$ = 351 nm, while the onset is determined at λ = 397 nm. It can be attributed to be the transition of π → π*.[14] Weaker absorption band is observed at λ = 305 nm, which is assigned to be the transition of δ → π.[15] A small bathochromic shift occurs in the solid state. The PL spectra in solution features the similar profiles with that of in film. The peak is located at ∼435 nm and the FWHM of 58 nm in solution and 46 nm in film, respectively. Moreover, the compound of **DPTPA** exhibits a pronounced
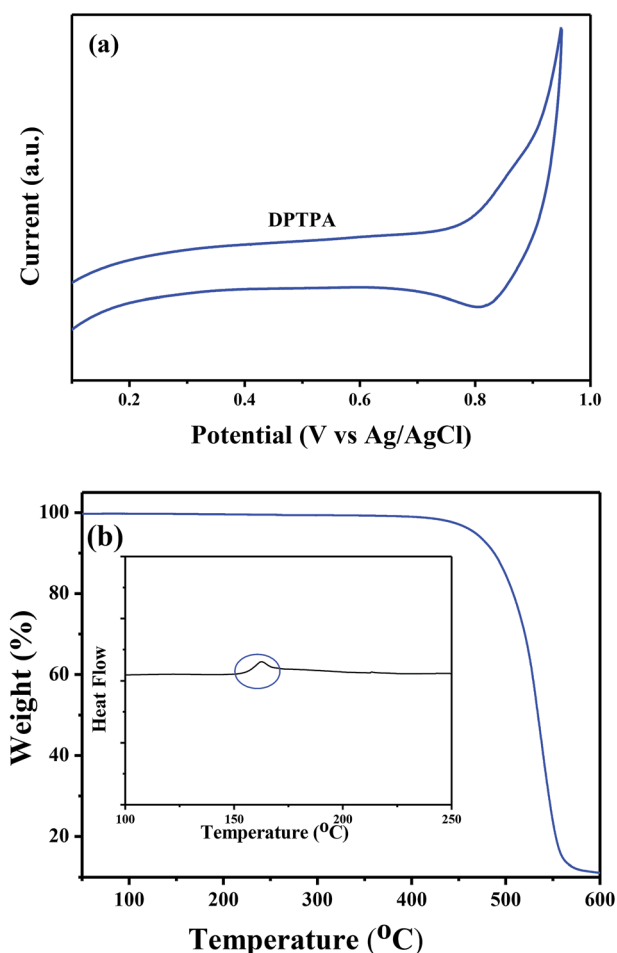
Table 1 Summaries of physical properties of DPTPA

| Abs[a] (nm)	PL[a] (nm)	T_g (°C)	$T_d{}^b$ (°C)	Φ^c (%)	Abs[d] (nm)	PL[d] (nm)	HOMO (eV[e], eV[f])	LUMO (eV[e], eV[f])	$E_g{}^g$ (eV)	$E_g{}^h$ (eV)
349	434	151	469	23.8	355	438	−5.26, −4.90	−2.11, −2.24	3.15	2.66

[a] UV-vis absorption and PL spectra in THF. [b] Loss of 5 wt%. [c] Measured by the integrating sphere system with neat film. [d] UV-vis absorption and PL spectra in neat film. [e] HOMO was measured from the onset of oxidation potential, LUMO was deduced from HOMO and E_g. [f] Obtained from DFT calculations using B3LYP/6-31G*. [g] Obtained from the onset of UV-vis absorption spectra in film. [h] Calculated from the HOMO and LUMO based on the calculations of B3LYP/6-31G*.
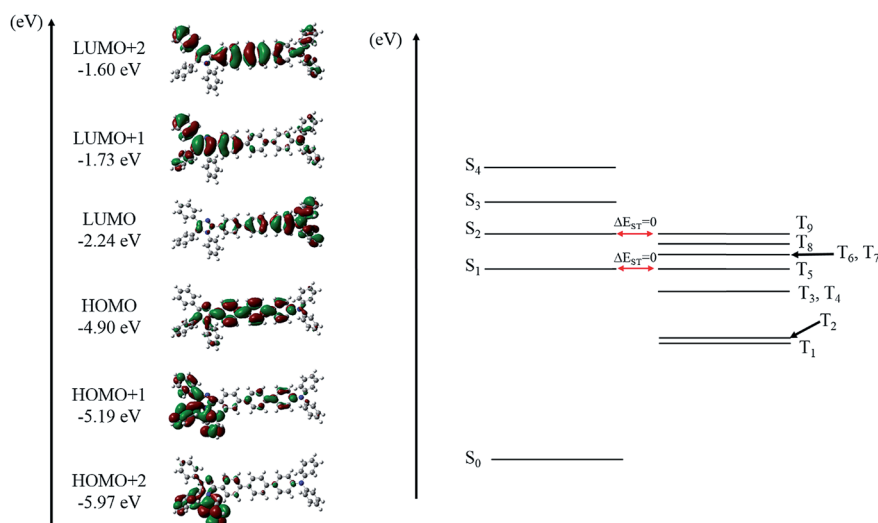
Fig. 3 Calculated energy levels, molecular orbitals, and excited state of DPTPA.

Stokes-shift by almost 80 nm, which is characteristic for a large reorganization in the excited state.[16] Additionally, the PL spectra in various polarity solvents were recorded and are shown in Fig. 5. With increase of the solvent polarity gradually from petroleum ether to acetonitrile, the PL spectra exhibit a larger red-shifted, broader shape. Obviously, a large difference in the dipole moment between the excited state and the ground state, the CT state with a large polarity is usually stabilized in polar solvents, and the change is consistent with a variety of the excited state from the LE-state to an excited state with the strong CT character.[17] The dipole moments were calculated according to the Lippert–Mataga theory to be 21.7 and 5.4 D, respectively.[18] The present results are very similar with the pioneer work by Ma and his colleagues.[19] Considering that the two compounds in this work have similar molecular structures, we can confirm these emitters also show the excited states of hybridized local and charge-transfer (HLCT). Furthermore, the phosphorescent spectra and PL decay characteristics were also investigated and the lifetimes of DPTPA was observed to be 1.49 ns, respectively, which could be assigned to the ordinary fluorescence.

2.5 Electroluminescent properties

To investigate DPTPA's electroluminescence (EL) characteristics as a saturated deep-blue emitter, a device with a configuration
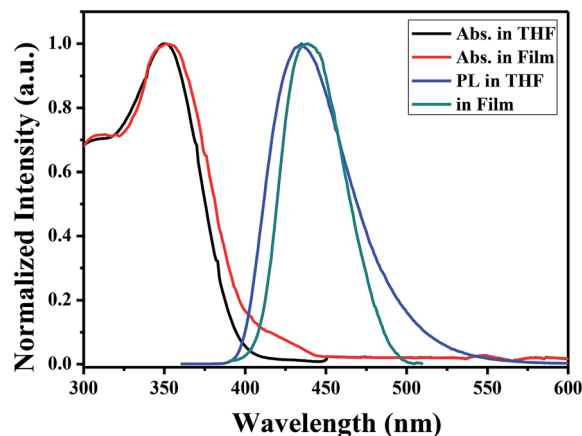
Fig. 4 The absorption and fluorescence spectra of DPTPA in THF solution and in a thin film.

of ITO/HAT-CN (5 nm)/NPB (40 nm)/TCTA (5 nm)/**DPTPA** (20 m)/TPBI (40 nm)/LiF (1 nm)/Al was fabricated. Here, ITO (indium tin oxide) and LiF/Al are the anode and the cathode, respectively; 4,4′-bis[N-(1-naphthyl)-N-phenylamino]biphenyl (NPB) and 1,3,5-tris(N-phenylbenz-imidazol-2-yl)benzene (TPBI) are employed respectively as the hole-transporting layer (HTL) and the electron-transporting layer (ETL); whereas, 4,4′,4″-
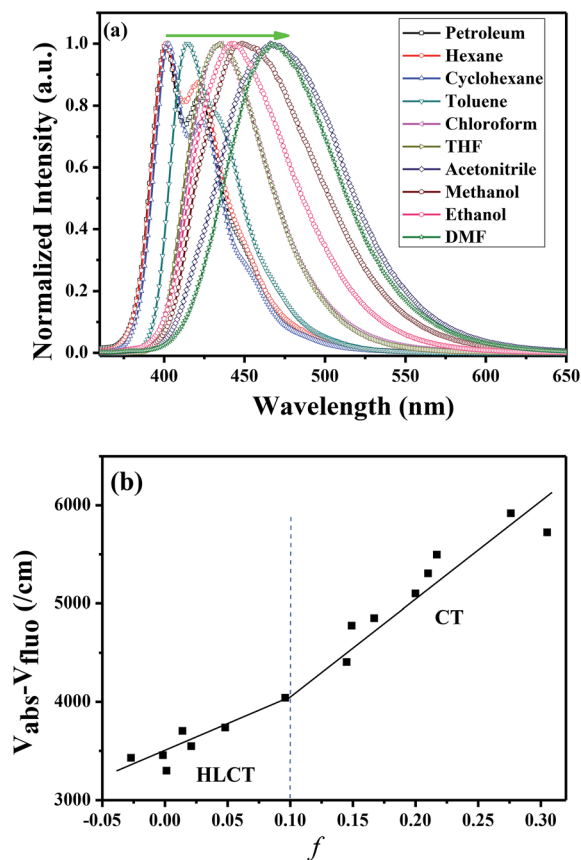
Fig. 5 (a) The fluorescence spectra of **DPTPA** in various polarity solvents; (b) linear correlation of the orientation polarization (Δf) of solvent media with the Stokes shift ($v_a - v_f$; a: absorbed light; f: fluorescence) for **DPTPA**. In low-polarity and high-polarity solvents, the S_1 state is the HLCT state and the CT state, respectively.

tris(*N*-carbazolyl)triphenylamine (TCTA) serves as the electron-blocking layer (EBL).

The electroluminescent (EL) spectra, current density–voltage–luminance (J–V–L) characteristics, and CE–current density–PE plots of the device based on **DPTPA** are shown in Fig. 6, and the key performance parameters of the device are summarized in Table 2. The device shows a saturated deep-blue emission solely from **DPTPA** (peaked at 438 nm) and Commission Internationale de L'Eclairage (CIE) coordinates of (0.15, 0.09). The EL spectra show little changes as the brightness increases from 10 to 10 000 cd m^{-2}. Furthermore, a low turn-on voltages (voltage required to give 1 cd m^{-2}) of 2.8 V was observed. The low turn-on voltages are mainly attributed to charge injection and balanced charge recombination in the emitter layer. For the EL efficiencies, the device exhibits impressive maximum EQE, CE and PE of 3.81%, 3.45 cd A^{-1} and 3.52 lm W^{-1}, respectively, and these efficiencies remain to be 3.78%, 3.43 cd A^{-1} and 3.12 lm W^{-1} at a brightness of 100 cd m^{-2}, even at the brightness of 1000 cd m^{-2}, these efficiencies still remain to be 3.40%, 3.07 cd A^{-1} and 1.88 lm W^{-1}. Considering the low fluorescent quantum yield (23.8%) and high device external quantum efficiency (3.81%), the performances are among the best for saturated deep-blue

fluorescent OLEDs.[20] The corresponding theoretical value of the radiative exciton ratio was calculated by the following equation: $\eta_{ext} = \gamma \eta_r \eta_{PL} \eta_{out}$, in which η_r is the radiative exciton ratio, η_{ext} is the external quantum efficiency, η_{out} is the light out-coupling efficiency (*ca.* 20%), η_{PL} is the intrinsic photo-luminescence efficiency (*ca.* 23.8%), and γ is the recombination efficiency of injected holes and electrons, which is ideally 100% only if holes and electrons are fully balanced and completely recombined to form excitons. Thus, the η_r value of the **DPTPA** device was calculated to be 80%, which breaks through the limit of the radiative exciton ratio of 25% for conventional FOLEDs. Since no delayed fluorescence was observed from transient PL, and the luminance of EL displayed a linear increase with increasing current density, the high radiative exciton ratio does not seem to be in accordance with some mainstream views, such as thermally activated delayed fluorescence (TADF) or triplet–triplet annihilation (TTA).[21,22]

The hybrid WOLED with the architecture of single-EML was fabricated with the same construction as the previous **DPTPA**-based device with the only difference that the **DPTPA** layer contains different concentration of Ir(2-phq)$_3$ from 0.1 to 0.9 wt%. As shown in Fig. 7a, all of devices with different concentration of Ir(2-phq)$_3$ are showing extremely low turn-on voltage of 2.6 V, and low driving voltages of 4.2 eV (0.1 wt%), 3.8 eV (0.3 wt%), and 3.5 eV (0.65 and 0.9 wt%) at a practical brightness of 1000 cd m^{-2}. The EL efficiencies are illustrated in Fig. 7b and c and listed in Table 2. When the concentration of Ir(2-phq)$_3$ is ∼0.9%, the hybrid WOLED exhibits maximum total EQE, CE and PE of 22.3%, 53.7 cd A^{-1} and 60.2 lm W^{-1}, respectively. As decrease of the concentration of Ir(2-phq)$_3$, the efficiencies reduce gradually. When the concentration of Ir(2-phq)$_3$ is down to 0.1%, the efficiencies are declined to be 13.2%, 25.8 cd A^{-1} and 29.1 lm W^{-1}, respectively, indicating that about 50% IQE could be harvested in this concentration. In Fig. 7d, a warm white light emission can be realized when the concentration of Ir(2-phq)$_3$ is up to 0.9 wt%. The corresponding CIE coordinates show a moderate blue shift from (0.51, 0.41) to (0.43, 0.34) when the brightness increases from 10 to 10 000 cd m^{-2}. While the doped concentration was decreased to 0.6 wt%, the CIE coordinates changed from (0.49, 0.40) to (0.39, 0.31), the present white emission is near to the standard white light at high brightness (ESI, S1†). When the concentration was down to 0.35 wt%, the CIE coordinates changed from (0.45, 0.36) to (0.29, 0.22), Thus, a cold white light can be obtained at high luminance (ESI, S2†). As the concentration is changed to be 0.1%, which is following the conventional principle of the doping concentration regulation, the present spectra cannot be found enough the emission from the phosphorescence even at the high luminance (ESI, S2†).

2.6 Discussion about exciton transfer mechanism in the high concentration of phosphorescent dopant

To clearly demonstrate the exciton transfer mechanism in the high concentration of phosphorescent dopant WOLEDs, we
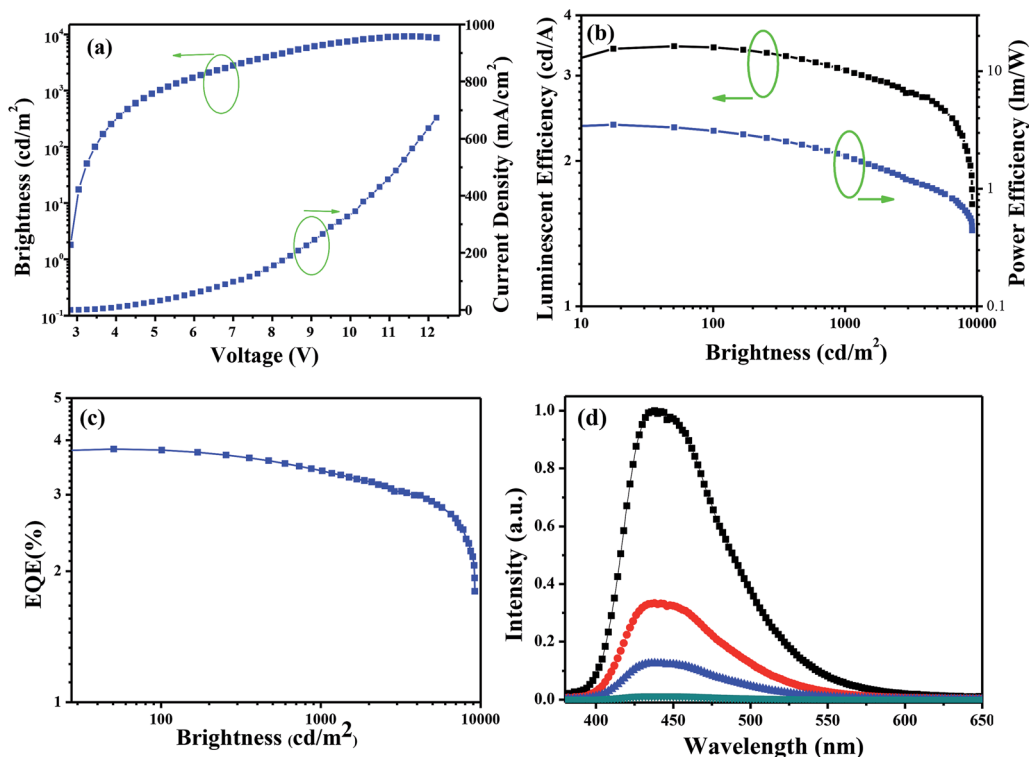
Fig. 6 The performance of device based on pure **DPTPA**, (a) the curves of voltage–brightness–current density; (b) the curves of brightness–luminescent efficiency–power efficiency; (c) the curve of brightness–EQE; (d) the electroluminescent spectra.

Table 2 Summary of device performance in correlation with the concentration of Ir(2-phq)$_3$

Doping concentration	V_{on}[a] (V)	CE$_{max}$ (cd A^{-1})	PE$_{max}$ (lm W^{-1})	EQE$_{max}$ (%)	At 100 cd m^{-2}					At 1000 cd m^{-2}				
					V (V)	CE (cd A^{-1})	PE (lm W^{-1})	CIE (x, y)	EQE (%)	V (V)	CE (cd A^{-1})	PE (lm W^{-1})	CIE (x, y)	EQE (%)
0	2.8	3.45	3.52	3.81	3.5	3.43	3.12	(0.15, 0.09)	3.78	5.1	3.07	1.88	(0.15, 0.09)	3.40
0.1	2.6	25.8	29.1	13.2	3.1	17.3	17.3	(0.28, 0.18)	10.9	4.2	10.7	7.99	(0.23, 0.16)	8.1
0.35	2.6	44.1	49.3	19.2	3.0	35.5	37.1	(0.41, 0.33)	16.5	3.8	21.8	17.8	(0.35, 0.28)	11.6
0.6	2.6	48.5	54.4	21.3	2.9	45.9	50.2	(0.48, 0.39)	20.0	3.5	32.6	28.9	(0.45, 0.36)	14.9
0.9	2.6	53.7	60.2	22.3	2.9	51.8	55.1	(0.50, 0.49)	21.9	3.5	38.3	33.2	(0.48, 0.38)	16.8

[a] At the luminance of 1 cd m^{-2}.

combined the results of theoretical calculations, monochromatic light devices and WOLEDs. Considering the improved dopant concentration in the single-EML-SD F/P hybrid WOLEDs, it is suspected that the current relatively high doping concentration should be resulted from the blue emitters with HLCT characters and thus "hot exciton" energy transfer from T$_5$ to S$_1$. Due to the part transfer from the triplet excited states to the singlet excited states of the blue emitter, the phosphorescent dopant cannot obtain sufficient energy to emit orange-red light of the traditional devices with the same doping concentration as shown in Fig. 8. At the 0.9 wt% doping concentration, the fluorescence emission utilize about ~60.8% excitons, and about 55% excitons are from the triplet state T$_5$ by hot-excitons process, while the excitons transferred

from singlets of the fluorescent to phosphorescent emitters can be calculated the ratio of their fluorescent lifetimes $(L_F/L_P = (\tau_F/\tau_P)^{0.5})$[23] in the mixed film, and the value from singlets of the fluorescent to phosphorescent emitters is 19.2%. The energy transfer from the triplet excited states of **DPTPA** to those of Ir(2-phq)$_3$ is found to be only 20%. Accordingly, a more than 55% of triplet excitons cannot transfer from **DPTPA** to Ir(2-phq)$_3$. It means that the insufficient energy can be transferred to the orange-red dopant, and the doping concentration should be improved to a high level. Furthermore, the present results can not only make the future mass production much easier to control accurately, but also a great breakthrough in the device mechanism, and then the design strategy.
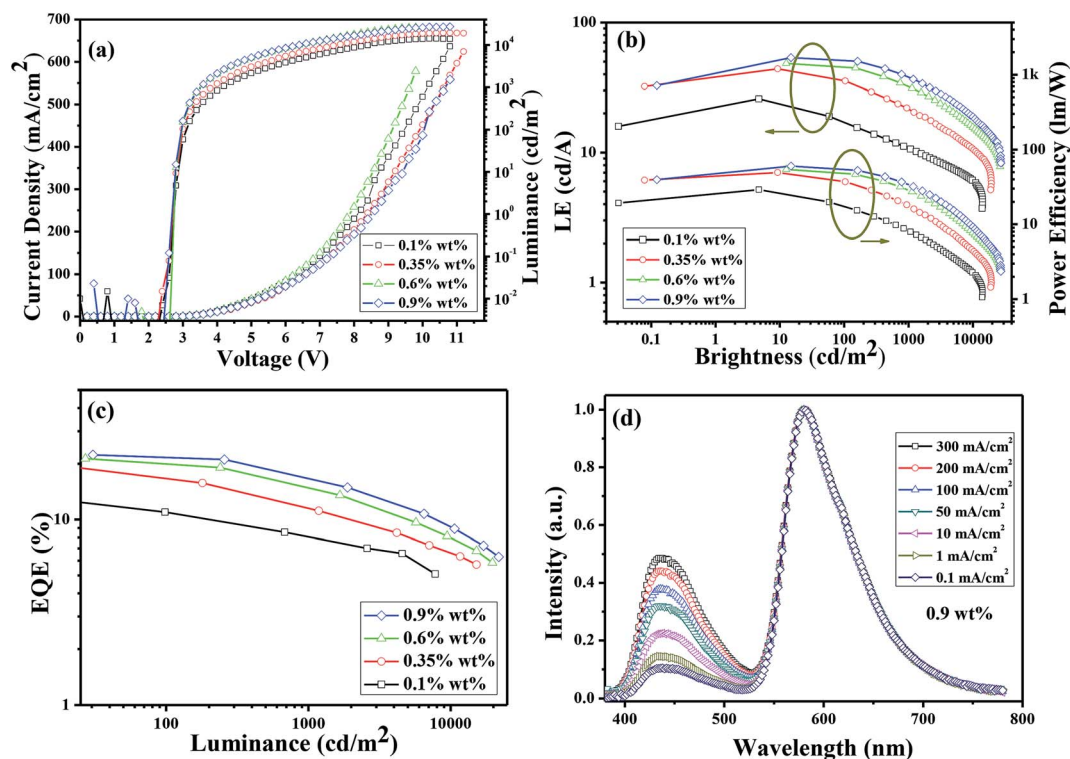
Fig. 7 (a) The current density−voltage−luminance curves; (b) the brightness−LE−power efficiency curves; (c) the luminance−EQE curve; and (d) the electroluminescent spectra of the concentration of 0.9 wt%.
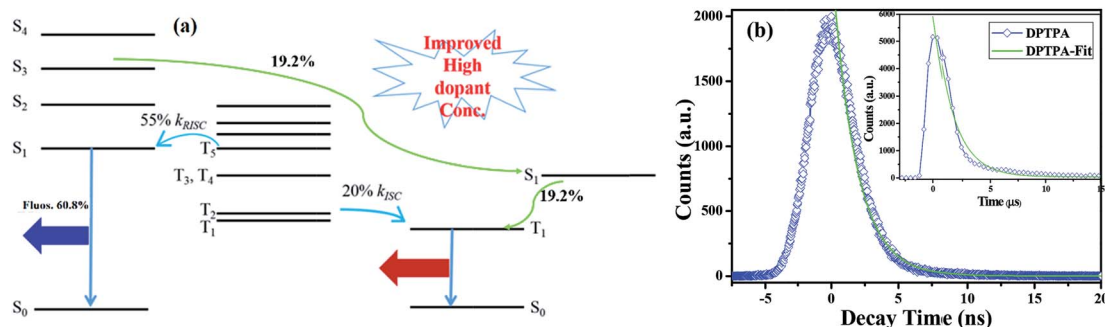

Fig. 8 (a) The illustration of exciton forming process of emitter from hole and electron recombination in electric excitation condition of WOLEDs; (b) the transient singlet PL of **DPTPA** films doped with 0.9 wt% of Ir(2-phq)$_3$, the corresponding transient triplet PL is shown in inserted figure.

3. Conclusions

In summary, we have presented a novel imidazole based emitter material for high-efficient fluorescent OLED and single-EML F/P hybrid WOLED devices. It is notable that the WOLED still exhibited white emission with a maximum total EQE, CE and PE of 22.3%, 53.7 cd A^{-1} and 60.2 lm W^{-1}, respectively, when the concentration of Ir(2-phq)$_3$ is up to 0.9 wt%, which is not following the conventional principle of the doping concentration regulation. The exciton transfer mechanism in the high concentration of phosphorescent dopant is also discussed. Meanwhile, the devices also showed low roll of with the efficiencies of 16.9%, 38.3 cd A^{-1} and 33.2 lm W^{-1} at 1000 cd m^{-2}, it is among the best results for EML-simplified F/P-WOLEDs. The studies provide a way to obtain high performance F/P hybrid WOLEDs with a simple architecture and high doping concentration for easily manipulation.

4. Experimental section

4.1 Synthesis

All reagents, unless otherwise specified, were obtained from Alfa Aesar or Sigma-Aldrich and used without further purification. Some of the solvents used were further purified before use (THF from sodium/benzophenone, methanol from CaH$_2$). ^{1}H and ^{13}C NMR spectra were measured using a Bruker AV-400. Chemical shifts were expressed in parts per million (ppm),

and splitting patterns are designated as s (singlet), d (doublet), m (multiplet) and br (broad). Coupling constants J are reported in Hertz (Hz). Elemental analyses were performed on a Vario EL elemental analysis instrument (Elementar Co.).

4.1.1 Synthesis of compound 2. (4-(Diphenylamino)phenyl) boronic acid (2.89 g, 10.0 mmol), 1-bromo-4-iodobenzene (1.415 g, 5 mmol) and Pd(PPh$_3$)$_4$ (50 mg, 0.1 mmol) were suspended in toluene (30 mL) and K$_2$CO$_3$ (10 mL of 2 M aqueous solution) and the reaction was stirred at 90 °C for 24 h. The orange solution was extracted with CH$_2$Cl$_2$ (40 mL × 3 times), washed with water (20 mL × 3 times), dried over MgSO$_4$ and evaporated to dryness. After drying under vacuum, it was purified by silica gel column chromatography using CH$_2$Cl$_2$–petroleum ether (60–90 °C) (1 : 15) as an eluent to afford a white solid, yield: 1.68 g, 84%. MS (EI): m/z 399.1, 401.3 (M$^+$), which was agreement with the literature.[1]

4.1.2 Synthesis of compound 3. Compound **2** (2 g, 5 mmol), 1-bromo-4-iodobenzene (0.75 g, 5 mmol) and Pd(PPh$_3$)$_4$ (50 mg, 0.1 mmol) were suspended in toluene (30 mL) and K$_2$CO$_3$ (10 mL of 2 M aqueous solution) and the reaction was stirred at 90 °C for 24 h. The orange solution was extracted with CH$_2$Cl$_2$ (40 mL × 3 times), washed with water (20 mL × 3 times), dried over MgSO$_4$ and evaporated to dryness. After drying under vacuum, it was purified by silica gel column chromatography using CH$_2$Cl$_2$–petroleum ether (60–90 °C) (1 : 1) as an eluent to afford a yellow solid, yield: 1.83 g, 86.1%. ^{1}H NMR (400 MHz, CDCl$_3$) δ 10.01 (s, 4H), 7.99 (d, J = 7.86 Hz, 2H), 7.83 (d, J = 8.42 Hz, 2H), 7.75–7.70 (m, 4H), 7.55 (d, J = 8.42 Hz, 2H), 7.32–7.28 (m, 5H), 7.19–7.16 (m, 5H), 7.07 (t, J = 7.86 Hz, 2H). MS (EI): m/z 425.2 (M$^+$).

4.1.3 Synthesis of compound DPTPA. A mixture of aniline (0.465 g, 5.0 mmol), benzil (0.21 g, 1.0 mmol), compound **3** (0.425 g, 1.0 mmol), ammonium acetate (0.308 g, 4.0 mmol), and acetic acid (10 mL) was refluxed under nitrogen in an oil bath. After 2 h, the mixture was cooled and filtered. The solid product was washed with an acetic acid–water mixture (1 : 1, 30 mL) and water. Then it was dried in the vacuum, the crude product was purified by silica gel column chromatography using CH$_2$Cl$_2$–petroleum ether (60–90 °C) (2 : 1) as an eluent to afford a yellow solid, yield: 0.613 g, 88.7%. ^{1}H NMR (400 MHz, CDCl$_3$) δ 7.65–7.64 (m, 6H), 7.57–7.52 (m, 6H), 7.35–7.21 (m, 13H), 7.17 (d, J = 8.42 Hz, 8H), 7.13–7.11 (m, 2H), 7.06 (t, J = 7.28 Hz, 2H). MS (EI): m/z 692.1. Anal. calcd for C$_{51}$H$_{37}$N$_3$: C, 88.54, H, 5.39, N, 6.07; found: C, 88.59, H, 5.22, N, 6.19%.

4.2 Devices fabrication and measurement

The EL devices were fabricated by vacuum deposition of the materials at 5×10^{-4} Pa or below onto ITO glass with a sheet resistance of 20 Ω per square. Before the fabrication of devices, the emitters of PhBPI and BBPI were purified deeply by sublimation. All of the organic layers were deposited at a rate of 1.0–2.0 Å s^{-1}. The cathode was deposited with LiF (1 nm) at a deposition rate of 0.1 Å s^{-1} and then capping with Al metal (100 nm) through thermal evaporation at a rate of 4.0 Å s^{-1}. The electroluminescence (EL) spectra were measured by a PR705 spectra scan spectrometer. The luminance–current density and voltage characteristics were recorded simultaneously with the measurement of Commission Internationale De L'Eclairage (CIE) coordination of these devices by combining the spectrometer CS200 with a Keithley model 2420 programmable voltage–current source. All measurements were carried out at room temperature under ambient conditions.

References

1 C. Fan and C. L. Yang, *Chem. Soc. Rev.*, 2014, **43**, 6439.

2 S. Lee, H. Shin and J.-J. Kim, *Adv. Mater.*, 2014, **26**, 5864.

3 D. D. Zhang, L. Duan, L. Li, D. Q. Zhang and Y. Qiu, *J. Mater. Chem. C*, 2014, **2**, 8191.

4 B. Pan, B. Wang, Y. X. Wang, P. Xu, L. Wang, J. S. Chen and D. G. Ma, *J. Mater. Chem. C*, 2014, **2**, 2466.

5 M. Vasilopoulou, D. Georgiadou, G. Pistolis and P. Argitis, *Adv. Funct. Mater.*, 2007, **17**, 3477.

6 C. L. Ho, L. C. Chi, W. Y. Hung, W. J. Chen, Y. C. Lin, H. Wu, E. Mondal, G. J. Zhou, K. T. Wong and W. Y. Wong, *J. Mater. Chem.*, 2012, **22**, 215.

7 N. Sun, Q. Wang, Y. B. Zhao, Y. H. Chen, D. Z. Yang, F. C. Zhao, J. S. Chen and D. G. Ma, *Adv. Mater.*, 2014, **26**, 1617.

8 P. F. Atkins, *Physical Chemistry*, Oxford University Press, Oxford, 4th edn, 2005.

9 J. Zhao, L. Liu, J. H. Wu and J. S. Yu, *Dyes Pigm.*, 2014, **102**, 234.

10 G. Schwartz, S. Reineke, T. C. Rosenow, K. Walzer and K. Leo, *Adv. Funct. Mater.*, 2009, **19**, 1319.

11 Y. T. Tao, Q. Wang, Y. Shang, C. L. Yang, L. Ao, J. G. Qin, D. G. Ma and Z. G. Shuai, *Chem. Commun.*, 2009, 77.

12 J. Ye, C. J. Zheng, X. M. Ou, X. H. Zhang, M. K. Fung and C. S. Lee, *Adv. Mater.*, 2012, **24**, 3410.

13 M. J. Frisch, G. W. Trucks, H. B. Schlegel, G. E. Scuseria, M. A. Robb, J. R. Cheeseman, J. A. Montgomery Jr, T. Vreven, K. N. Kudin, J. C. Burant, J. M. Millam, S. S. Iyengar, J. Tomasi, V. Barone, B. Mennucci, M. Cossi, G. Scalmani, N. Rega, G. A. Petersson, H. Nakatsuji, M. Hada, M. Ehara, K. Toyota, R. Fukuda, J. Hasegawa, M. Ishida, T. Nakajima, Y. Honda, O. Kitao, H. Nakai, M. Klene, X. Li, J. E. Knox, H. P. Hratchian, J. B. Cross, V. Bakken, C. Adamo, J. Jaramillo, R. Gomperts,

R. E. Stratmann, O. Yazyev, A. J. Austin, R. Cammi, C. Pomelli, J. W. Ochterski, P. Y. Ayala, K. Morokuma, G. A. Voth, P. Salvador, J. J. Dannenberg, V. G. Zakrzewski, S. Dapprich, A. D. Daniels, M. C. Strain, O. Farkas, D. K. Malick, A. D. Rabuck, K. Raghavachari, J. B. Foresman, J. V. Ortiz, Q. Cui, A. G. Baboul, S. Clifford, J. Cioslowski, B. B. Stefanov, G. Liu, A. Liashenko, P. Piskorz, I. Komaroni, R. L. Martin, D. J. Fox, T. Keith, M. A. Al-Laham, C. Y. Peng, A. Nanayakkara, M. Challacombe, P. M. W. Gill, B. Johnson, W. Chen, M. W. Wong, C. Gonzalez and J. A. Pople, *Gaussion 03, Revision A1*, Gaussian, Inc., Pittsburgh, PA, 2003.

14 X. H. Ouyang, X. Y. Zhang and Z. Y. Ge, *Dyes Pigm.*, 2014, **103**, 39; T. L. Wu, H. H. Chou, P. Y. Huang, C. H. Cheng and R. S. Liu, *J. Org. Chem.*, 2014, **79**, 267.

15 T. L. Wu, H. H. Chou, P. Y. Huang, C. H. Cheng and R. S. Liu, *J. Org. Chem.*, 2014, **79**, 267.

16 L. Yao, S. T. Zhang, R. Wang, W. J. Li, F. Z. Shen, B. Yang and Y. Ma, *Angew. Chem., Int. Ed.*, 2014, **53**, 2119.

17 P. Zhang, W. Dou, Z. H. Ju, L. Z. Yang, X. L. Tang, W. S. Liu and Y. Z. Wu, *Org. Electron.*, 2013, **14**, 915.

18 C. J. Chiang, A. Kimyonok, M. K. Etherington, G. C. Griffiths, V. Jankus, F. Turksoy and A. P. Monkman, *Adv. Funct. Mater.*, 2013, **23**, 739.

19 W. J. Li, D. D. Liu, F. Z. Shen, D. G. Ma, Z. M. Wang, T. Femg, Y. X. Xu, B. Yang and Y. G. Ma, *Adv. Funct. Mater.*, 2012, **22**, 2797.

20 H. J. Liang, X. X. Wang, X. Y. zhang, Z. Y. Liu, Z. Y. Ge, X. H. Ouyang and S. D. Wang, *New J. Chem.*, 2014, **38**, 4696.

21 Q. S. Zhang, L. Jie, K. Shizu, S. P. Huang, S. Hirata, H. Miyazaki and C. Adachi, *J. Am. Chem. Soc.*, 2012, **134**, 14706.

22 J. Y. Hu, Y. J. Pu, F. Satoh, S. Kawata, H. Katagiri, H. Sasabe and J. Kido, *Adv. Funct. Mater.*, 2014, **24**, 2064.

23 S. Chandrasekhar, *Rev. Mod. Phys.*, 1943, **15**, 1.